

Image-Based Simulations Show Important Flow Fluctuations in a Normal Left Ventricle: What Could be the Implications?

C. CHNAFA,^{1,2} S. MENDEZ,¹ and F. NICLOUD¹

¹Université de Montpellier - IMAG CNRS UMR 5149, Place Eugene Bataillon, 34095 Montpellier Cedex 5, France; and
²Biomedical Simulation Laboratory, University of Toronto - Mechanical and Industrial Engineering, 5 King's College Road, Toronto, ON M5S 3G8, Canada

(Received 12 January 2016; accepted 6 April 2016)

Associate Editor Umberto Morbiducci oversaw the review of this article.

Abstract—Intra-cardiac flow has been explored for decades but there is still no consensus on whether or not healthy left ventricles (LV) may harbour turbulent-like flow despite its potential physiological and clinical relevance. The purpose of this study is to elucidate if a healthy LV could harbour flow instabilities, using image-based computational fluid dynamics (CFD). 35 cardiac cycles were simulated in a patient-specific left heart model obtained from cardiovascular magnetic resonance (CMR). The model includes the valves, atrium, ventricle, papillary muscles and ascending aorta. We computed phase-averaged flow patterns, fluctuating kinetic energy (FKE) and associated frequency components. The LV harbours disturbed flow during diastole with cycle-to-cycle variations. However, phase-averaged velocity fields much resemble those of CMR measurements and usually reported CFD results. The peak FKE value occurs during the E wave deceleration and reaches 25% of the maximum phase-averaged flow kinetic energy. Highest FKE values are predominantly located in the basal region and their frequency content reach more than 200 Hz. This study suggests that high-frequency flow fluctuations in normal LV may be common, implying deficiencies in the hypothesis usually made when computing cardiac flows and highlighting biases when deriving quantities from velocity fields measured with CMR.

Keywords—Left heart, MRI, Transitional flow, Turbulence, LES, Turbulent kinetic energy, Mitral valve, Atrium, Third sound, Bruit.

INTRODUCTION

The hemodynamics of the left ventricle (LV) conveys useful information regarding the heart func-

tion.^{25,40} Therefore, direct observation of LV flow patterns or indirect measurements of the flow through LV bruits or ejection fraction may signal a normal LV or reflect the presence of an installed pathology. In addition to indicating an abnormal function, there is substantial evidence that the LV hemodynamics can be responsible for the initiation of ventricular remodelling through mechanical stimuli.^{12,36} Indeed, LV adaptations involve mechanosensitive feedbacks, which modulate cardiomyocytes architecture and thus cardiac function.³⁸ Therefore, accurate assessment of the intraventricular flow from smallest to largest scales is of paramount importance to get further comprehension of the role played by the hemodynamics in normal and abnormal LV.

Previous *in vivo* studies of 4D intra-cardiac flows have been heavily based on filtered velocity data obtained thanks to phase-contrast cardiovascular magnetic resonance (CMR)³² imaging. Although comprehensive, CMR velocity mapping is not real-time, but rather measure an averaged heart cycle. Hence, cycle-to-cycle variations and instabilities in the flow cannot be recorded, as the *k*-space is filled over many cardiac cycles.^{15,32} Moreover, CMR spatio-temporal resolution precludes the observation of small-scale and fast time-varying flow features in the case of disturbed flow.

Used with caution, image-based computational fluid dynamics (CFD) offers a research tool³⁹ able to retrieve all the scales of the instantaneous flow, hence being able to capture highly disturbed flows. However, pioneering CFD studies focused only on the laminar features of the flow.^{24,29,47,48,52} While these studies retrieve the large-scale flow features, they were not able to detect fluctuations as such features are likely to be damped by the numerical setup employed.⁵⁰ To the best of our knowledge, apart from our previous

Address correspondence to C. Chnafa, Biomedical Simulation Laboratory, University of Toronto - Mechanical and Industrial Engineering, 5 King's College Road, Toronto, ON M5S 3G8, Canada. Electronic mail: cchnafa@mie.utoronto.ca

80 study,¹⁰ only Le and Sotiropoulos²⁸ have mentioned
81 flow fluctuations in a patient-specific LV model (al-
82 though without quantifications) and Domenichini
83 *et al.*¹³ mentioned that in certain conditions LV could
84 be on the edge of “turbulence”.

85 We emphasise that in addition to be controversial, the
86 nature of the flow in normal heart most probably does
87 not comply with the canonical definition of developed
88 turbulence. Due to the flow nature, the Kolmogorov
89 energy cascade does not have time to establish,⁴³ making
90 the definition of intracardiac turbulence problematic.
91 Nevertheless, non-periodic, 3D fluctuations may appear
92 given the Reynolds number of order 5000, the flow do-
93 main complexity and the pulsatile nature of the flow. In
94 the present study, irrespective of the exact nature of the
95 flow, we are referring to cycle-to-cycle flow fluctuations
96 simply as “fluctuations” and we are defining the flow as
97 “disturbed” or “transitional”.

98 Despite its potential importance, little focus has
99 been directed on the disturbed nature of the LV flow.
100 The intrinsic technical limitations of the CMR exams
101 or the numerical strategies generally employed in LV
102 CFD studies are likely to be responsible for the quasi-
103 absence of studies about fluctuations, as they cannot
104 grasp the entire nature of the flow. Fluctuations were
105 reported in our previous studies^{9,10} in an abnormal
106 heart and very recently, using a new CMR method to
107 evaluate the intensity and the localization of velocity
108 fluctuations, Zajac *et al.*⁵³ confirmed the presence of
109 non-negligible *in vivo* level of “turbulent” kinetic en-
110 ergy in abnormal and normal LVs. As the nature of the
111 flow directly affects the characteristic time scales and
112 local levels of flow stresses, we believe that the analysis
113 of the velocity fluctuations can provide a new para-
114 digm in the assessment of the cardiovascular flow and
115 mechanosensitive feedbacks. In addition, characteriz-
116 ing fluctuations might give potential explanation to
117 heart sounds.⁴⁶ In this paper we are using image-based
118 simulations¹⁰ to address the question of whether or not
119 fluctuations are detected in a normal LV. The impli-
120 cations of their existence are then discussed.

121 MATERIALS AND METHODS

122 In this study, a subject-specific left heart (LH) model
123 and its deformation were extracted from CMR acqui-
124 sitions. Computational fluid dynamics (more precisely
125 large-eddy simulations) was used to study the flow in
126 this model.

127 *Patient-Specific Domain*

128 CMR images were obtained from a healthy subject
129 of 26 years old. The 4D image set consists in 20 three-

dimensional images of spatial resolution 130
131 $5.0 \times 1.1 \times 1.1 \text{ mm}^3$, which correspond to
132 $21 \times 256 \times 256$ voxels. The subject cardiac cycles
133 lasted on average $T = 750 \text{ ms}$. We selected one 3D
134 image (referred to as the *native* image) at an arbitrary
135 moment of the heart cycle and we imported the cor-
136 responding volumetric data into an image processing
137 software (ScanIP; Simpleware Ltd., Exeter, UK). We
138 segmented a 3D domain covering all the space occu-
139 pied by blood in the LH cavities using a thresholding
140 method and a smoothing procedure.⁴² Figure S01 in
141 the supplementary materials shows a long axis slice of
142 the CMR exam and the segmentation resulting from
143 the thresholding method. The 3D domain includes the
144 ventricle, atrium, four pulmonary veins, the ascending
145 aorta and the papillary muscles. We chose to simulate
146 the entire LH, even if the focus is on the LV, in order
147 to mitigate the uncertainty related to the swirled and
148 skewed flow at the mitral valve (MV).^{10,34} Figure 1
149 shows the domain used for the CFD. The extracted
150 geometry was imported in a mesh generator (Gambit,
151 ANSYS) to generate the grid of the *native* numerical
152 domain.

153 A set of numerical treatments was applied to the
154 CMR images and the *native* grid in order to generate a
155 time-varying computational domain representing the
156 physiological deformations of the LV. The resulting
157 LV volume (as defined in Fig. 1 i.e., the LV volume is
158 delimited by the AO and MV annulus) varies from
159 109 mL (end diastolic volume) to 41 mL (end systolic
160 volume). The stroke volume is 68 mL and the ejection
161 fraction is 62%, which falls within the normal physi-
162 ological range.³¹ Details are provided in previous
163 studies.^{9,10}

164 The aortic valve (AV) and the MV are difficult to
165 extract from the medical images as they are thin and
166 highly moving structures. However, as valves have an
167 impact on the flow structure,⁵ low-order models were
168 included in the domain. The valve models have been
169 described in detail in a previous work^{9,10} and are only
170 briefly recalled here. Annuluses are reconstructed by
171 inspecting the medical images and placing markers
172 manually on the *native* 3D domain. The motion of
173 these markers is then obtained thanks to the heart
174 motion extracted from the medical images. We mod-
175 elled the AV, which has a moderate impact on the
176 ventricular flow, as a planar region at the AV annulus
177 being alternatively permeable and impermeable
178 depending on the phase in the cardiac cycle. We
179 modelled the MV using parameters measured in the
180 CMR exam: the leaflet length, annulus position and
181 MV open area. Figure S02 in the supplementary
182 materials depicts the measurements of the mitral open
183 area and the measurements along the diastole. The
184 median opened area is $A_{MV} = 5.18 \text{ cm}^2$, which falls in

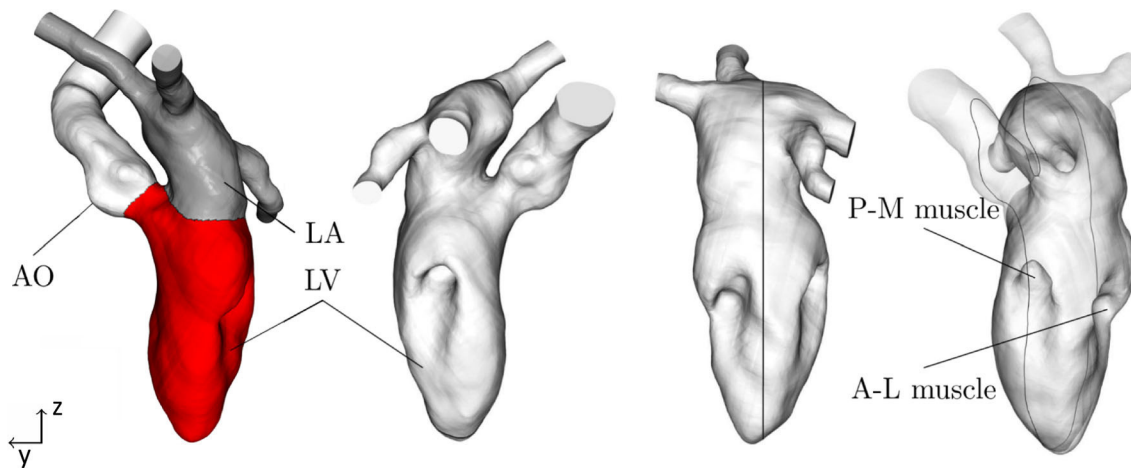


FIGURE 1. Full human LH extracted from CMR images. The same domain is shown from four different points of view. The inlets and outlet flow extensions are visible in the left figure. The left ventricle (LV), left atrium (LA), Aorta (AO), Antero Lateral (A-L) and Postero Medial (P-M) papillary muscles are indicated. A black line passing through the LH indicates the position of the slice which will be used to display the velocity field in the next section. The red volume is the volume used for all the volumetric integrations over the LV. The volume is delimited by the aortic and mitral annulus.

185 the normal physiological range.³¹ The open area
 186 available for the fluid flow is modelled as an ellipse of
 187 axis $a = 15$ mm and $b = 11$ mm. Knowing the MV
 188 leaflets position during the heart cycle, their effect on
 189 the blood flow is accounted for by using an immersed
 190 boundary method.⁹ For this purpose, the leaflets rep-
 191 resentations are given a thickness so that a few mesh
 192 nodes are located within the valves. Then, the fluid
 193 velocity is imposed to zero within the leaflets.

194

Fluid Boundary Conditions

195 A no-slip condition was applied to the moving heart
 196 walls. The inflow boundary conditions at the pul-
 197 monary veins were computed by assuming that the
 198 mitral and aortic valves are either closed-open or open-
 199 closed at each instant. Under this assumption, the flow
 200 rate entering the flow domain is related to the time
 201 evolution of either the atrium volume or the atrio-
 202 ventricular volume, by using the mass conservation
 203 principle. In other words, the boundary conditions are
 204 derived from the medical images⁹ and the associated
 205 heart deformations over time. The resulting waveform
 206 is applied as a boundary condition at the four pul-
 207 monary veins, assuming an equipartition between the
 208 four inlets. The same inlet waveform and wall defor-
 209 mation are applied for each cycle, precluding the
 210 generation of cycle-to-cycle variations into the flow
 211 through boundary condition. A traction free outflow
 212 condition is applied at the outlet. Figure 2 displays the
 213 resulting flow rates at the AV and the MV.

214 The E wave peak ($0.57 T$) corresponds to an
 215 entering flow rate of 365 mL s^{-1} in the ventricle. The
 216 A wave peak occurs at $0.89 T$ and corresponds to an

entering flow rate of 180 mL s^{-1} resulting in a E/A 217
 ratio of 2. The maximum Reynolds is $Re = 4524$ at the 218
 MV tips using the area A_{MV} , the effective mitral mean 219
 diameter $D = 2\sqrt{A_{MV}/\pi}$, the maximum flow rate and 220
 a constant kinematic viscosity $\nu = 4.0 \times 10^{-6} \text{ m}^2 \text{ s}^{-1}$. 221
 The Stokes number is $\beta = D^2 \nu T = 220$ and the 222
 Strouhal number is $St = \beta/Re = 0.049$. Table 1 sum- 223
 marizes the main characteristics of the simulation 224
 compared to normal values. 225

Numerical Setup

226

227 The Navier–Stokes equations (NS) are solved using
 228 large-eddy simulations and the finite-volume method
 229 as implemented in the YALES2BIO solver^{10,33}
 230 (www.math.univ-montp2.fr/~yales2bio). The YALES2 231
 solver and its biomechanical spin-off YALES2BIO 232
 have been extensively validated in prior studies. Simple 233
 and idealized geometries have been used to validate the 234
 solver and can be found here.⁸ The code has shown its 235
 capability to reproduce accurately industrial configu- 236
 ration against another CFD code and against experi- 237
 mental measurements *via* Particle Image Velocimetry 238
 (PIV).¹ Moreover, Toda *et al.*² studied the accuracy of 239
 the LES model we are using in this study thanks to an 240
 experimental setup of a pulsatile jet impinging a flat- 241
 plate in the presence of a cross-flow. This configuration 242
 shows a strong similarity with the mechanisms present 243
 in the heart and reported in the present study. Toda 244
*et al.*² showed the capability of the LES model in 245
 reproducing accurately this experimental configuration 246
 against PIV.

247 The code uses spatial gradients computed with a
 248 centred fourth-order scheme. The time-advancement

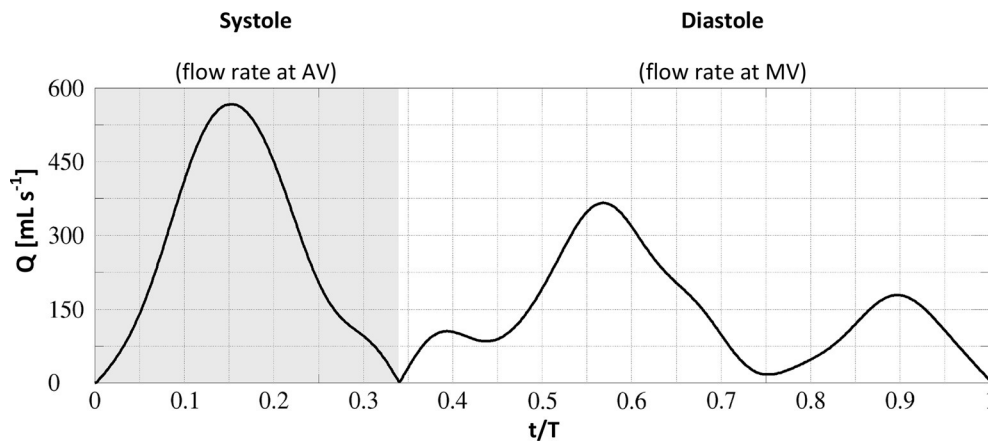


FIGURE 2. Flow rates at the aortic valve (null during diastole) and at the mitral valve (null during systole). The grey area delimits the systolic phase from 0 to 0.34 T. Note that a normal time ratio of one-third (systole) to two-thirds (diastole) is respected.

TABLE 1. Main flow characteristics of the LV simulated compared to LV normal ranges.

	Present simulation	Normal range
Heart rate (beat min ⁻¹)	85	60–100
E/A ratio	2.0	1.0–2.0
EDV (mL)	109	65–240
ESV (mL)	41	16–143
SV (mL)	68	55–100
Cardiac output (L min ⁻¹)	5.8	4.0–8.0
Ejection fraction (%)	62	55–70
MV Open area (cm ²)	5.18	4.0–6.0
U_{\max} at MV (m s ⁻¹)	0.7	0.6–1.0
Re_{\max} at MV	4524	4146–5642

The range of the Reynolds number is computed from U_{\max} , using the normal range of the MV open area, and the viscosity used in the simulation ($\nu = 4.0 \times 10^{-6} \text{ m}^2 \text{ s}^{-1}$).

EDV: end-diastolic volume; ESV: end-systolic volume; SV: stroke volume.

249 scheme of the NS equation is an explicit low-dissipa-
 250 tive, low-storage, four-step Runge–Kutta scheme re-
 251 cast in an arbitrary Lagrangian–Eulerian formalism.
 252 The pressure term is treated with the Chorin’s projec-
 253 tion-correction method. We modelled the subgrid-
 254 scales with the Sigma eddy-viscosity model.³⁵ We dis-
 255 cretized the LH geometry using ten million tetrahedral
 256 elements. The average edge length of the tetrahedra
 257 was close to 0.55 mm during diastole. See Fig S03 in
 258 the supplementary materials for a representation of the
 259 computational mesh. The time step calculation was
 260 based on a Courant–Friedrichs–Lewy stability number
 261 of 0.9, which resulted in a temporal resolution varying
 262 from 0.2 ms during the beginning of diastole to 0.5 ms
 263 during diastasis. Five cycles were simulated to wash
 264 out the initial conditions and statistics were accumu-
 265 lated over 30 additional cycles.

266 As a common practice when using properly resolved
 267 LES, all quantities are computed from the resolved

velocity field in this study.^{4,43} We note that during our
 268 computations the sub-grid scale viscosity remains low
 269 in the LV during the whole the heart cycle, showing
 270 that the sub-grid scale model dissipates a moderate
 271 amount of energy. Figure S04 (supplementary materi-
 272 als) shows the ratio between the sub-grid scale viscosi-
 273 ty and the fluid viscosity. As expected, the sub-grid scale
 274 viscosity is virtually zero during the systole and has
 275 moderate values, but non-null, during the most tur-
 276 bulent part of the cycle. The maximum mean ratio is
 277 approximatively 0.2 during the more turbulent part of
 278 the cycle. To go further, an estimation of the Pope
 279 criterion⁴⁴ can be computed as $k_{\text{sgs}}/k \approx 3C\Delta k/2\pi L$ ⁴³
 280 where $C = 1.5$, $\Delta = 0.55 \text{ mm}$ and, $L = 0.04 \text{ m}$ being
 281 the characteristic length of the largest structures. For
 282 the present LES, $k_{\text{sgs}}/k = 6\%$ which remains three
 283 times below the 15–20% threshold usually used to
 284 evaluate if a LES is sufficiently resolved.⁴⁴
 285

286 RESULTS

287 General Flow Features Within the Left Ventricle

288 Figure 3 displays phase-averaged flow velocity
 289 solutions projected onto the slice indicated in Fig. 1.
 290 Atrium and aorta are displayed, but the description
 291 focuses on the LV flow. As flow patterns in ventricles
 292 are dominated by the diastolic inflow, we only show
 293 salient moments of the diastolic phase.

294 During the E wave filling, a jet enters the ventricle
 295 and generates a vortex ring, quickly regionally con-
 296 strained due to its interaction with the LV surface. The
 297 vortex ring becomes asymmetric: the unconstrained
 298 part of the vortex moves and grows as shown by the
 299 velocity field plotted at 0.65 T. Therefore, at the end of
 300 the E wave, the initial vortex ring forms a recirculating
 301 cell, as shown by the velocity field plotted at 0.75 T,

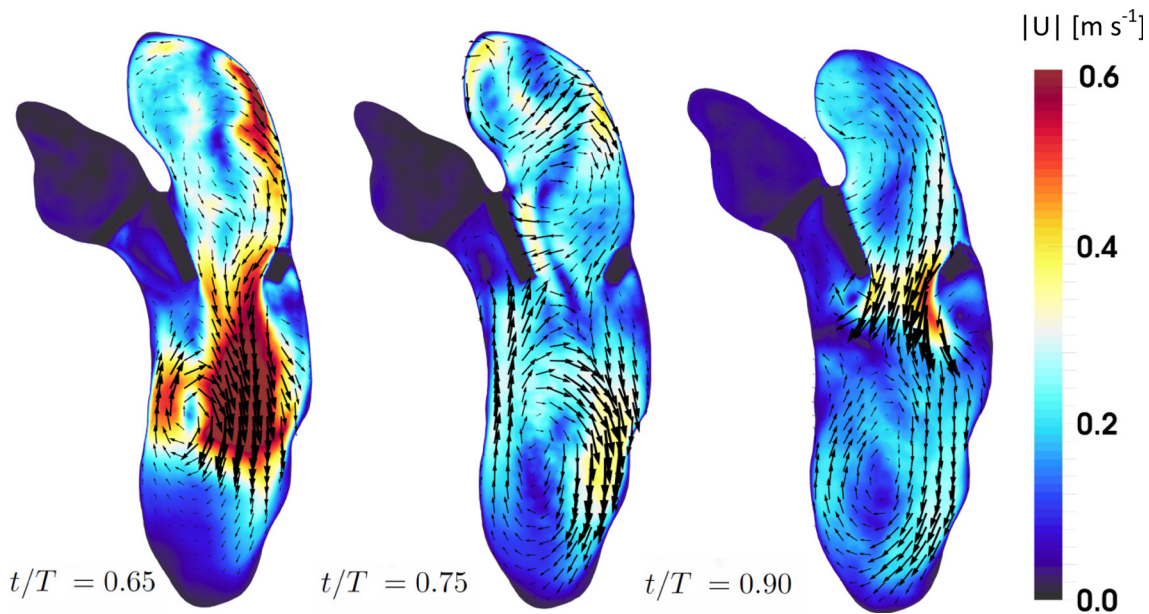


FIGURE 3. Phase-averaged diastolic velocity field over a cutting plane through the LH (see Fig. 1 for the plane position). The MV and the AV are depicted in black. Colour map represents the velocity magnitude. The velocity vectors are plotted each 3.7 mm. The figure shows the classically reported structure of the LV diastole: the E wave vortex ring during the second half of the E wave filling (0.65 T), the recirculating cell during the diastasis (0.75 T) and the A wave filling (0.9 T).

302 which takes up the entire ventricle for the rest of the
 303 cycle. After diastasis, at 0.9 T, a new jet enters the
 304 ventricle as displayed in the right figure. This second
 305 injection of fluid corresponds to the A wave. This
 306 vortex ring is less intense than the E wave vortex and
 307 remains more coherent, as it does not impinge with the
 308 heart wall. At the end of diastole, the MV closes and
 309 the AV opens. The systolic phase begins; the ventricle
 310 volume decreases and blood is ejected from the LV.
 311 Overall, the simulation retrieves the classically
 312 reported large-scale flow structures.^{26,32,51}

313 In addition, small-scale structures are present in the
 314 LV, but they are not visible on the phase-averaged
 315 fields. Figure 4 displays instantaneous velocity solu-
 316 tions at 0.75 T (left and middle plots) for two consec-
 317 utive heart cycles while the right plot shows the phase-
 318 averaged flow for the same time (also displayed in
 319 Fig. 3). Instantaneous velocity solutions exhibit cycle-
 320 to-cycle fluctuations, looking like random flow varia-
 321 tions in time and space, mainly from the impingement
 322 of the E wave vortex ring (at roughly 0.65 T) to the end
 323 of diastole. Cycle-to-cycle differences are visible in the
 324 entire LH while the phase-averaged flow (right plot)
 325 shows the large-scale features usually reported in
 326 *in vitro*, *in silico* and *in vivo* studies.

327 Regional Repartitions of the Fluctuations in the LV

328 In order to study the regional distribution and
 329 quantify these fluctuations we computed the difference

between the phase-averaged velocity components U_i 330
 and the instantaneous velocity components u_i ($i = 1, 2,$ 331
 3). The fluctuating part of the fluid velocity is, 332

$$u'_i = U_i - u_i, \quad 333$$

and we defined the fluctuating kinetic energy (FKE) 335
 per unit volume as, 336

$$\text{FKE} = \frac{\rho}{2} \langle u'_i u'_i \rangle,$$

where $\langle \cdot \rangle$ denotes phase-averaged values, and with 338
 implicit sum. Figure 5 displays the FKE in the LV 339
 when the vortex ring interaction with the heart wall 340
 occurs (left figure), during diastasis (centre figure) and 341
 at the A wave peak (right figure). 342

343 We also provide an animation of the volumetric
 344 rendering of the FKE in the LV during the heart cycle,
 345 as supplementary online material. During the heart
 346 cycle, the FKE ranges from zero to 150 J m^{-3} in the
 347 LV. Fluctuations around 60 J m^{-3} are observed in the
 348 vortex ring and its wake. The highest FKE values are
 349 predominantly located in the basal region, in the upper
 350 third of the LV, when the vortex ring begins to interact
 351 with the heart wall at $\sim 0.62 \text{ T}$. After this interaction,
 352 fluctuations are visible in the major part of the LV,
 353 while their intensity decreases throughout the rest of
 354 the cycle. Values under 10 J m^{-3} are mainly detected
 355 in the LV apical area. Later during the cycle, fluctua-
 356 tions are generated in the wake of the A wave vortex
 357 ring and remain in the basal region. Fluctuations are
 358 dissipated during systole.

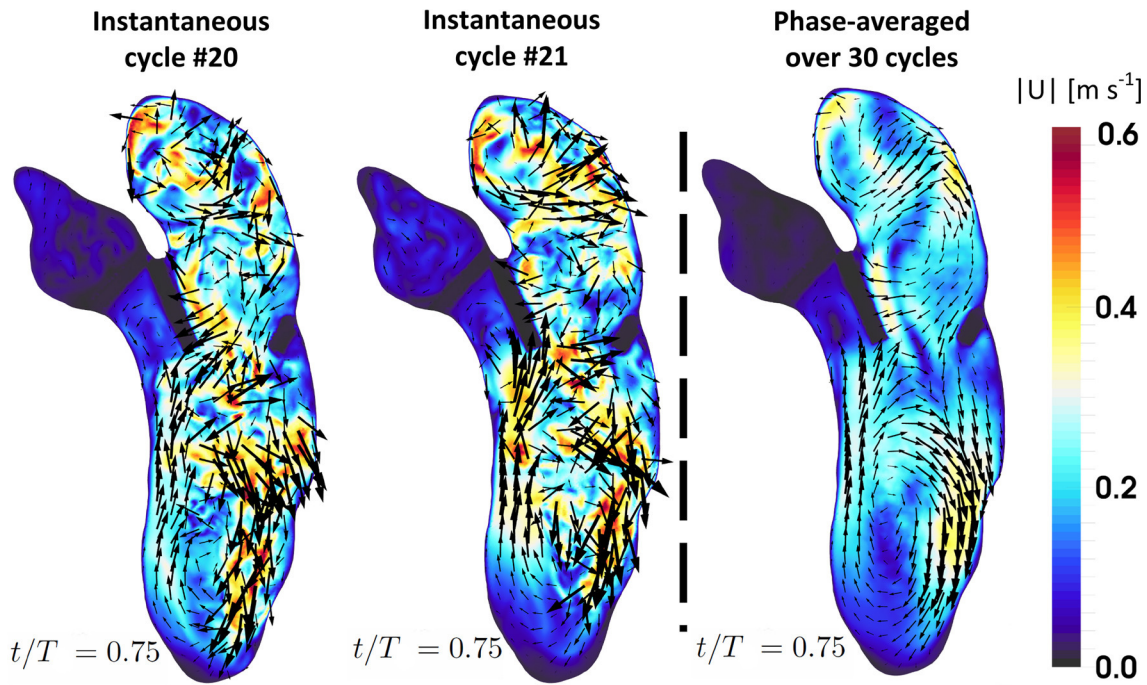


FIGURE 4. Left and middle plots: instantaneous velocity fields at 0.75 T for two consecutive heart cycles. Right plot: phase-averaged velocity field over thirty heart cycles at 0.75 T. Note the large cycle-to-cycle fluctuations while the phase-averaged flow shows the classically reported flow pattern.

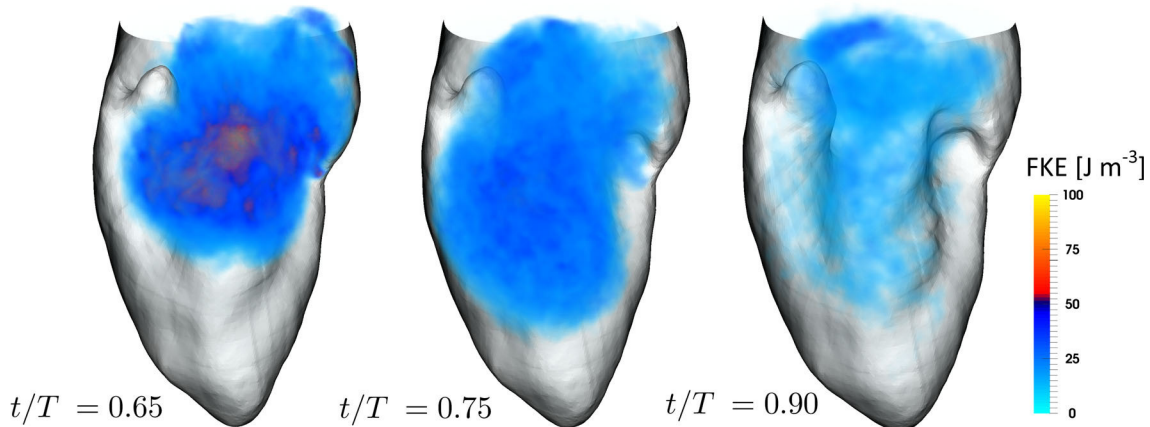


FIGURE 5. 3D volume rendering of the FKE in the LV during the second half of the E wave peak (left, 0.65 T), diastasis (middle, 0.75 T) and at the A wave peak (right, 0.9 T). The opacity is set to 0% for FKE values below 10 J m^{-3} and then grows linearly from 0 to 100% for the maximum FKE values displayed.

359

Time-Frequency Analysis of the Fluctuations

360

361

362

363

364

365

366

367

368

In order to describe the energetic distribution of the fluctuating part of the velocity u'_i over the different flow frequencies, we computed spectrograms for different locations in the LV. Spectrograms have been preferred to the energy-frequencies study since the flow is here non-ergodic and highly transient, which precludes the *classic* use of such approach. We decomposed each velocity signal in 800 windows, applied a Hann window with 50% overlapping and used a short-

time Fourier transformation. The resulting spectrograms are then phase-averaged over the 30 cycles.

Spectrograms computed with different overlapping and window functions displayed only small differences,

which guarantee that the following results are robust to the details of the signal processing. Figure 6 displays the computed spectrograms at three Eulerian locations for the fluctuating energy.

The diastolic flow features broad ranges of frequencies at probes p_1 and p_2 while p_3 location displays

369

370

371

372

373

374

375

376

377

378

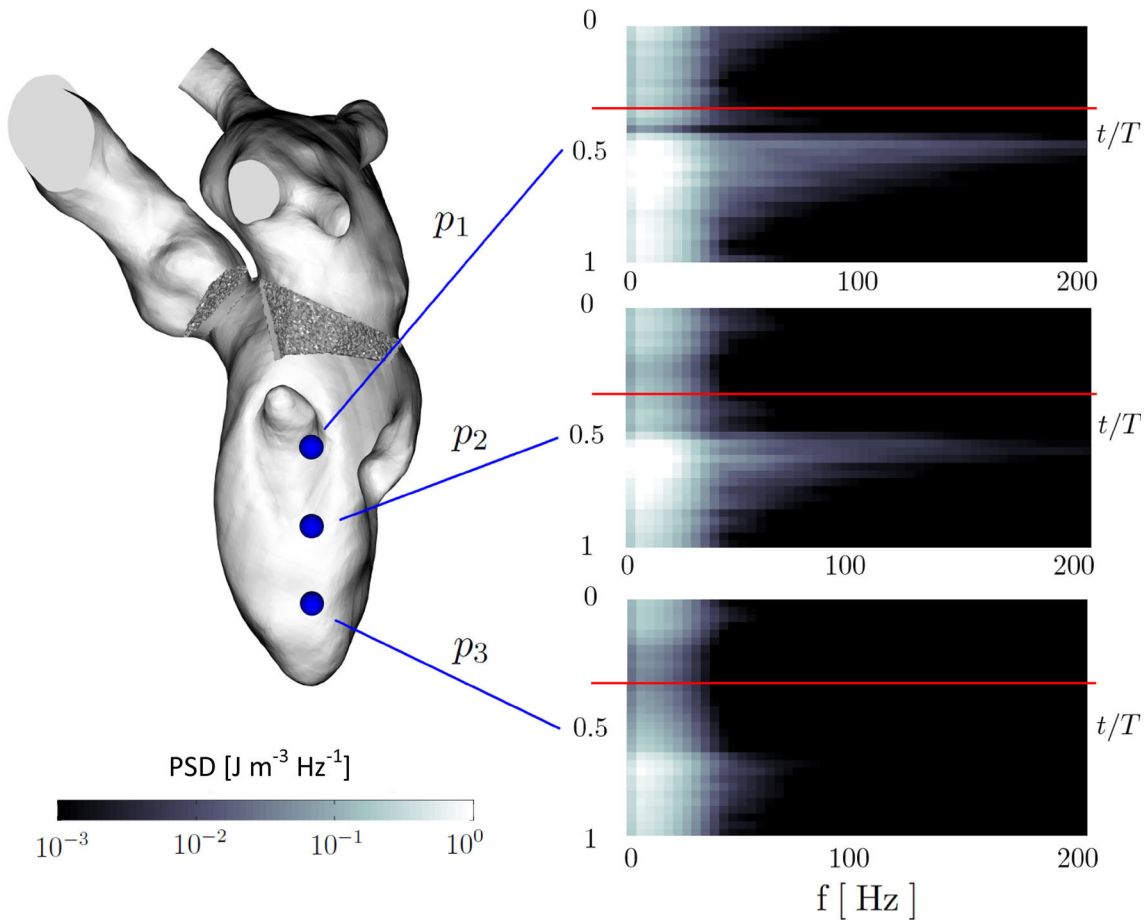


FIGURE 6. Time–frequency representation of the Power Spectral Density (PSD) in log scale of the velocity fluctuations u' at three locations. Each horizontal slice of a spectrogram exhibits the frequency spectrum of the flow at a specific time. Red lines on spectra delimit systole from diastole. The LH is made transparent. Atrium, open mitral valve and closed aortic valve are displayed. The three Eulerian probes p_1 , p_2 and p_3 are located as shown in the left hand side view (blue spheres).

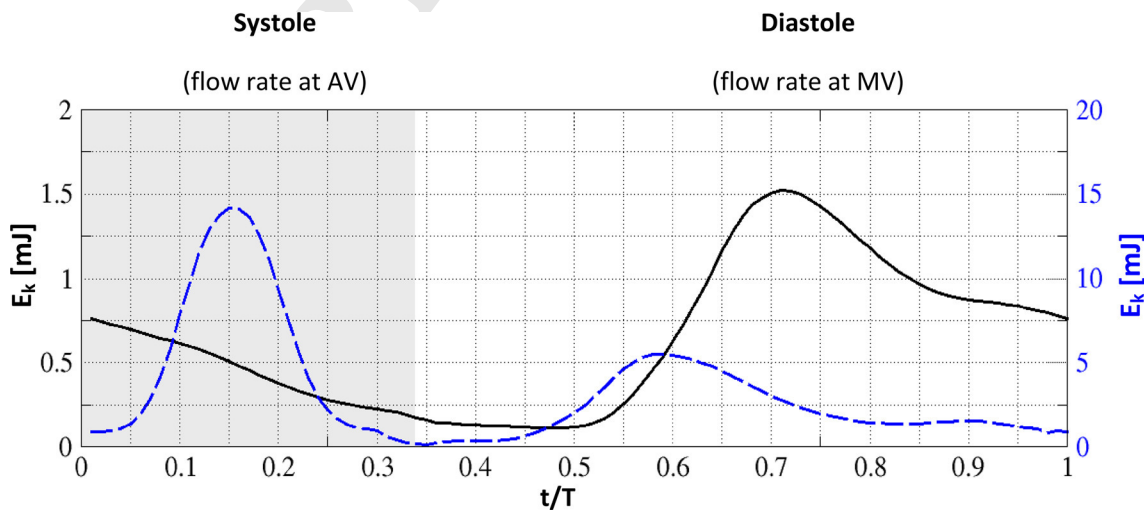


FIGURE 7. Fluctuating (black solid line) and averaged (blue dashed line) velocity kinetic energy integrated over the LV during a heart cycle.

379 lower frequencies. During the first half of diastole, the
 380 energy in the LV rises and is transferred from lower to
 381 higher frequencies. At location p_1 , the broader range of
 382 frequencies occurs at roughly 0.65 T, while the maxi-
 383 mum is reached at 0.77 T for p_2 and 0.9 T for p_3 . The
 384 frequency content of the fluctuations is in a range of
 385 frequencies up to 200 Hz for p_1 , 180 Hz for p_2 and
 386 70 Hz for p_3 . For the three locations p_1, p_2, p_3 , beside
 387 the short time windows when higher frequencies were
 388 visible, more than 95% of the energy remains con-
 389 centrated in frequencies lower than 35 Hz.

390 *Integrated Fluctuating Kinetic Energy*

391 Figure 7 displays the FKE and the averaged veloc-
 392 ity kinetic energy, integrated over $V(t)$, the time vary-
 393 ing volume of the LV. The volume $V(t)$ is delimited by
 394 the AO and MV valve annulus as shown in Fig. 1. We
 395 defined the integrated FKE as,

$$E_k(t) = \frac{\rho}{2} \int_{V(t)} \langle u'_i u'_i \rangle dV,$$

396 And the integrated average flow kinetic energy as,

$$E(t) = \frac{\rho}{2} \int_{V(t)} \langle U_i U_i \rangle dV.$$

402 E_k ranges from 0.1 to 1.5 mJ. During diastole, the
 403 increase of E_k measured throughout the LV chamber is
 404 associated with the beginning of the E wave. The FKE
 405 energy reaches its peak value during the inflow decel-
 406 eration at 0.71 T, occurring 0.12 T after the E wave
 407 peak. The E wave peak energy of the phase-averaged
 408 flow has an energy of 5.5 mJ, which falls into the range
 409 of measurements reported with CMR.^{3,23} The amount
 410 of FKE decreases during the rest of the diastole with a
 411 slight inflexion occurring during the last third of the A
 412 wave. The relaminarization continues during systole
 413 while a peak of averaged velocity energy occurs be-
 414 cause of the flow ejection through the aortic valve.
 415 Note that this peak seems 3–4 times higher than the
 416 values reported with CMR.^{3,23} We stress that in con-
 417 trast to E_k or, the diastolic peak of E , the peak value of
 418 E during systole is sensitive to the choice of volume of
 419 integration. As a sensitivity study, we integrated the
 420 energies with different volumes to show that the sys-
 421 tolic peak show the same values as reported with
 422 CMR^{3,23} when the aortic root is not considered in the
 423 integration. See Fig. S05 of the supplementary mate-
 424 rials.
 425

426 *Impact of the Fluctuations on the Wall Shear Stress*

427 In order to demonstrate the consequence of these
 428 fluctuations on a hemodynamic factor, we computed

the wall shear stress (WSS) in the LV for two consec- 429
 430 utive cycles and for the phase-averaged velocity field.
 431 This estimation is a first approximation since the sur-
 432 face of the ventricle is simplified. The WSS was com-
 433 puted as the multiplication of the total fluid stress and
 434 the surface traction vector.⁶ Figure 8 shows the
 435 resulting patterns over a part of the LV inner surface
 436 during diastasis. Cycle-to-cycle differences are impor-
 437 tant in term of patterns and local intensity while the
 438 phase-averaged pattern is more evenly distributed. The
 439 magnitude of the phase-averaged WSS falls into pre-
 440 viously reported range in the LV.³⁷

441 DISCUSSION

442 *Summary*

443 The LV large-scale flow features we described i.e.,
 444 the blood ejection, the two vortex rings for the E and A
 445 waves and the recirculating cell, are in accordance with
 446 the numerous observations performed *in vivo*,^{26,32} *in*
 447 *silico*^{13,34} and *in vitro*.^{19,45} However, our computation
 448 reveals also large velocity fluctuations, which are usu-
 449 ally not reported *in silico* but which are in line with the
 450 results of previous experimental work that used both
 451 simplified ventricle geometries and inflow boundary
 452 condition.^{14,45} The presence of these fluctuations is due
 453 to the conjunction of the complex geometry of the LV,
 454 the *high* Reynolds number of the E wave jet and several
 455 normal and known mechanisms of the diastolic flow:

- the shear layer instabilities of the Kelvin–Helmholtz type generated by the jets during the E and A wave, 456–458
- the interaction between the E wave vortex ring and the wall of the ventricle, 459–460
- the flow decelerations associated with an adverse pressure gradient after each filling wave, which favours flow instabilities. 461–463

464 Consequently, the velocity fluctuations are observed
 465 during diastole, primarily when the E wave jet impacts
 466 the heart wall and during the subsequent flow decel-
 467 eration. During systole, the fluid undergoes an accel-
 468 eration that dampens flow instabilities. The overall
 469 quantification of the fluctuations indicates a clear
 470 scenario: the flow presents several regimes from lami-
 471 nar, to transitional if not turbulent, at each heartbeat.
 472 The fluctuations during the transient phase are not
 473 negligible: during diastole, the peak ventricle-averaged
 474 FKE value occurring during the E wave deceleration
 475 reaches 25% of the maximum phase-averaged flow
 476 kinetic energy.

477 The fluctuations are not restrained to a specific
 478 location and are observed in the whole ventricle.

479 However, their intensity and range of frequency vary
 480 in space. They exhibit low intensity and limited fre-
 481 quency range in the apex area while they show high
 482 intensity and broader range of frequencies in the first
 483 third of the LV during 30% of the diastole. Should it
 484 be recalled, these fluctuations are just and only due to
 485 the non-linearity of the flow equations since the com-
 486 putational domain and boundary conditions are fully
 487 periodic in this study.

488 *Relationship with Previous In Silico Studies*

489 Despite never being studied, direct or indirect evi-
 490 dence of flow instabilities in LV has been previously
 491 reported. Today, the research tool most capable of
 492 detecting and characterizing instabilities in the heart is
 493 computational fluid dynamics. However, to the best of
 494 our knowledge, the only patient-specific studies evok-
 495 ing fluctuations are ours in a heart with restrictive
 496 filling^{9,10} and a study by Le and Sotiropoulos²⁸ who
 497 mentioned “transitions to a weak turbulent state” after
 498 the impingement of the E wave vortex ring, without
 499 further analysis. In an idealized geometry, Domeni-
 500 chini *et al.*¹³ mentioned that for a Strouhal number of
 501 $St = 0.05$ and a Stokes number of $\beta = 81$ the flow
 502 undergoes a transition to a weak turbulent regime in
 503 their simulation. They added that a decrease of the
 504 Strouhal number, especially with large Stokes number,
 505 could trigger a transition to a turbulent regime. Our
 506 results confirm their statement, considering the present
 507 patient-specific model corresponds to a Strouhal
 508 number of $St = 0.0486$ and a Stokes number of
 509 $\beta = 220$ during the E wave.

510 The scarcity of reports of fluctuations using CFD is
 511 actually not surprising. The majority of the pioneering
 512 LV CFD used low resolutions in space and/or dissipa-
 513 tive numerical schemes, which can spuriously elimi-
 514 nate flow fluctuations. We stress that in addition to
 515 using fourth-order, non-dissipative schemes, the num-
 516 ber of elements used for the present simulation is
 517 comparable to recent studies using direct numerical
 518 simulations^{34,51} and two to three orders of magnitude
 519 larger than the other pioneering studies avail-
 520 able.^{24,29,47,48,52} These observations call into question
 521 the underlying idea of laminar flow in the LV. Indeed,
 522 we think that the main reason why reports of flow
 523 instabilities are rare in the LV CFD literature is the
 524 widely held conception that healthy LV flows are
 525 laminar. Undeniably, irrespective of flow phenotype,
 526 main large-scale hemodynamic features, namely jets,
 527 recirculating cell, and ejection can be retrieved. How-
 528 ever, transient or turbulent state features small-scales
 529 phenomena that cannot be retrieved under the laminar
 530 hypothesis. Therefore, as shown recently in aneurysms
 531 CFD by Valen-Sendstad & Steinman,⁵⁰ our results

suggest that the laminar assumption often made 532
 implicitly, should be reconsidered in LV CFD if one 533
 wants to simulate all the flow features. 534

Relationship with Previous In Vivo Measurements 535

536 It is worth noting that any CFD study where flow
 instabilities are not properly represented cannot ad- 537
 dress the prevalence of ventricular bruits and mur- 538
 murs.^{31,46} Among the sounds usually reported, the S_3 539
 bruit is a low-frequency brief sound harbouring a main 540
 frequency content in the range of 10–100 Hz²² and 541
 occurring at the end of the E wave, 120–200 ms after 542
 the start of the diastole.^{11,22} Although the genesis of 543
 this sound is controversial, it is widely reported that 544
 “vibrations” occurring during the deceleration of the E 545
 wave generate this sound.^{20,27} These “vibrations” may 546
 be generated by the interaction of the flow instabilities 547
 with the LV tissue. 548

549 The fluctuations measured in the present study
 match the characteristics of the third sound S_3 . While 550
 we do not directly prove that the reported fluctuations 551
 are responsible for the S_3 bruit, extrapolation from our 552
 results would support a cause-and-effect relationship.⁴⁶ 553
 Indeed, the present time–frequency analysis showed 554
 consistent results regarding (a) the S_3 main frequency 555
 content previously reported²² (10–100 Hz) as well as 556
 (b) the time window when the most intense fluctuations 557
 occurred^{11,22} (120–200 ms). These observations sup- 558
 port the fact that the hemodynamic fluctuations 559
 reported in this paper are a plausible physical expla- 560
 nation for the S_3 bruit. 561

562 Furthermore, if this sound is induced by the inter-
 action of the flow instabilities and the LV tissue, it 563
 suggests that flow fluctuations are widespread in nor- 564
 mal LV. Collins *et al.*¹¹ showed on a large cohort that 565
 the S_3 bruit was detected in one third of asymptomatic 566
 individuals younger than 40. Note that their technic 567
 was not able to detect quiet or intermittent S_3 , 568
 underestimating potentially the already high preva- 569
 lence of this sound. 570

571 Recently, Dyverfeldt *et al.*¹⁸ developed a new tech-
 nique using CMR allowing the detection of velocity 572
 fluctuations and the estimation of their associated en- 573
 ergy *in vivo*. Zajac *et al.*⁵³ applied this technique on 574
 normal and myopathic LV and highlighted that the 575
 level of flow instabilities could be a relevant biomarker 576
 of abnormal flows in the ventricle. However, less in- 577
 tense fluctuations were also measured in normal ven- 578
 tricles. The fluctuations were observed in the basal 579
 third of the LV, with peaks associated with highest 580
 inflow velocity, i.e., peak E and peak A wave. For 581
 normal subjects, they reported a maximum of kinetic 582
 energy of 2.5 ± 1.2 mJ during diastole, which agree 583

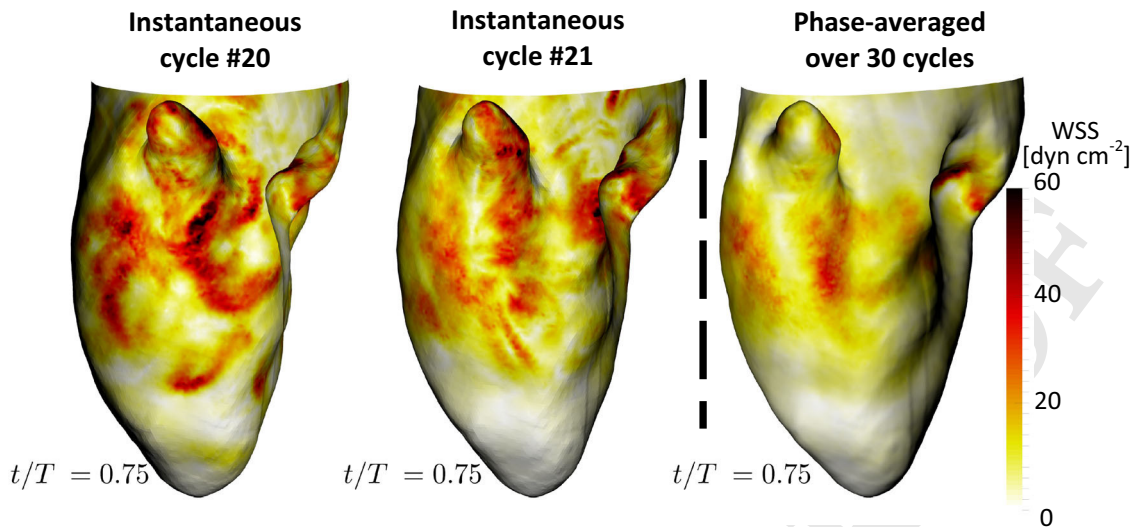


FIGURE 8. Left and middle plots: instantaneous wall shear stress maps at 0.75 T for two consecutive heart cycles. Right plot: phase-averaged wall shear stress map over 30 heart cycles at 0.75 T. Note the large cycle-to-cycle differences.

584 with the maximum value of 1.5 mJ obtained from our
585 computation.

586 *Potential Clinical Implications*

587 As shown by Zajac *et al.*⁵³ a certain level of fluctua-
588 tions intensity can be a sign of cardiac dysfunction.
589 It is actually commonly accepted that flow fluctuations
590 are synonym of pathologies in the cardiovascular sys-
591 tem.^{18,31} In light of the clinical observations discussed
592 above and our results, it seems that non-negligible
593 fluctuations in LV flows are actually not a synonym of
594 pathological flow. Flow fluctuations in normal LV
595 may be more common than thought so far, even
596 though their intensity are an order of magnitude lower
597 than the fluctuations found in the pathological cardio-
598 vascular flow previously reported.^{16,17} In other
599 words, the presence of flow fluctuations may reflect an
600 altered LV function but should not be systematically
601 considered as an absolute proof of a pathological state.

602 As CMR is widely used to explore the LV flow, the
603 prevalence of fluctuations in normal LV serves as a
604 reminder that time-resolved velocity fields measured
605 with CMR are not instantaneous but *mean* flow
606 fields.¹⁵ The blood flow patterns,⁴⁹ blood residence
607 times²¹ or any other quantity computed thanks to
608 velocity gradients (pressure difference, vorticity, wall
609 shear stress) correspond to the *mean* flow fields, not the
610 actual *in vivo* flow. While the same mean flow as CMR
611 is retrieved, Fig. 4 illustrates how different the
612 instantaneous flow may be. The wall shear stress maps
613 in Fig. 8 illustrate the consequences of these fluctua-
614 tions on the cycle-to-cycle forces experienced by the
615 heart cells.

616 Rather than the simple idea that fluctuations are a
617 sign of pathology, we suggest that conclusions also
618 depend on the levels of the fluctuations: flow fluctua-
619 tions with significant energy content would indicate
620 that substantial energy is transferred to fluctuations
621 and thus results in a loss of energy. However, some
622 fluctuations may be present, with small energy content,
623 as in the present study: the energy loss due to “tur-
624 bulence” is then small. In addition, to place the
625 intensity and duration of the fluctuations in perspec-
626 tive, a rapid analysis shows that these fluctuations
627 should not trigger blood damages. Consider first that
628 the components of the fluctuations are similar in
629 magnitude in all three directions, i.e., $u'_1 \approx u'_2 \approx u'_3$
630 $\approx u'$. This assumption allows writing $\text{FKE} \approx \frac{3\rho}{2} \langle u'^2 \rangle =$
631 $\frac{3}{2} \sigma_{\text{Reynolds}}$. The maximum FKE in the LV reached
632 locally 150 J m^{-3} , as described in the “Regional
633 Repartitions of the Fluctuations in the LV” section,
634 which corresponds to an estimated maximum Rey-
635 nolds stress component of 100 J m^{-3} . This value is
636 several times lower than the threshold values com-
637 monly cited for hemolysis,³⁰ especially for such a short
638 exposure time. Some fluctuations may actually even be
639 beneficial, especially during diastasis, to prevent the
640 increase of effective viscosity due to aggregation at low
641 shear rates.⁷ These fluctuating velocities amplify the
642 forces exerted by the blood on the LV wall cells, as
643 shown by Fig. 8, and can potentially trigger
644 mechanosensitive feedbacks. It has been shown *in vitro*
645 that even weak flow stimuli can induce modifications
646 of gene expression^{12,36} which in the LV, may result in
647 its functional modification. Although the remodelling
648 mechanisms of the LV are not completely understood

649 and that the relevance of these fluctuating velocities
 650 compared with the *mean* flow field remains to be de-
 651 fined, fluctuations can be expected to play an impor-
 652 tant role in myocardial function and adaptations.³⁸
 653 Such fluid dynamic considerations point toward
 654 interesting directions for future clinical research,
 655 complementing conventional studies focusing on the
 656 *mean* flow field.⁴¹

657 Limitations

658 An obvious limitation of our study is that we only
 659 simulate the LV of one subject under several modelling
 660 hypotheses and thus can only comment on the fluctu-
 661 ations detected in this simulation. Nevertheless, the
 662 results of this study are in accordance with several
 663 *in vivo*, *in silico* and *in vitro* evidence, as discussed
 664 above, and constitute a first step toward the study of
 665 these detected instabilities.

666 Some simplifications were also made. First, blood is
 667 here considered as Newtonian, as generally done in
 668 simulations of flows in large vessels. We did not
 669 account for the impact of the chordae tendineae of the
 670 MV or the trabeculations of the LV as they could not
 671 be captured by the CMR. These features could influ-
 672 ence the dissipation of the instabilities.⁵¹ The MV
 673 leaflet dynamics is not modelled: it may be speculated
 674 that their physiological flapping movement could en-
 675 hance instabilities because of the added vortex shed-
 676 ding⁵ while the widening of the MV could decrease the
 677 flow rate coming in the LV, decreasing the generation
 678 of instabilities. The degree to which our MV model will
 679 modulate the turbulence characteristics can hardly be
 680 judged.

681 The medical images and the registration algorithm
 682 pilot the deformations of our image-based LV. Thus,
 683 any images or registration flaws have an influence on
 684 the CFD results. A weak peak is visible on the MV
 685 flow rate at the very beginning of diastole: the quality
 686 of the CMR exam made it difficult for the registration
 687 algorithm to converge, generating indirectly this spu-
 688 rious peak. However, it can be speculated that this
 689 imperfection should have a limited impact on the
 690 presented results as the integrated FKE (Fig. 7) does
 691 only show a very weak inflexion corresponding to this
 692 event.

693 To be fully converged, the FKE statistics would
 694 need more cycles. However, a look at the computed
 695 FKE point-wise show that its cycle-averaged value
 696 using 20 or 30 cycles varies only by a few percent when
 697 the flow is the most disturbed. Figure S06 and Table S1
 698 in the supplementary materials show it. Thus, while
 699 admittedly not fully converged, the statistics were
 700 judged sufficiently converged to conduct our study.

701 Finally, we also did not consider the impact of beat-
 702 to-beat variations of the heart rate as the LV defor-
 703 mation was extracted from CMR. However, taking
 704 into account for such variations would most probably
 705 enhanced the cycle-to-cycle fluctuations observed in
 706 this study where the boundary conditions and heart
 707 deformations are periodic in time.

ELECTRONIC SUPPLEMENTARY MATERIAL

708
 709
 710 The online version of this article (doi:
 711 [10.1007/s10439-016-1614-6](https://doi.org/10.1007/s10439-016-1614-6)) contains supplementary
 712 material, which is available to authorized users.
 713

ACKNOWLEDGMENTS

714
 715 The authors would like to express their gratitude to
 716 MD Dr. D. Coisne for many fruitful discussions. Dr.
 717 R. Moreno from the Rangueil University Hospital,
 718 Toulouse (France) is acknowledged for the CMR ex-
 719 ams. Dr. V. Moureau and Dr. G. Lartigue from the
 720 CORIA lab, and the SUCCESS scientific group are
 721 acknowledged for providing the YALES2 code, which
 722 served as a basis for the development of YALES2BIO.
 723 This work was performed using HPC resources from
 724 GENCI-CINES (Grants 2014- and 2015-c20140371
 725 94).
 726

REFERENCES

- 727
 728
 729
 730
 731
 732
 733
 734
 735
 736
 737
 738
 739
 740
 741
 742
 743
 744
 745
 746
 747
 748
 749
 750
 751
 752
- ¹Barré, D., M. Kraushaar, G. Staffelbach, V. Moureau, and L. Y. M. Gicquel. Compressible and low Mach number LES of a swirl experimental burner. *Comptes Rendus Mécanique* 341:277–287, 2013.
 - ²Baya Toda, H., O. Cabrit, K. Truffin, G. Bruneaux, and F. Nicoud. Assessment of subgrid-scale models with a large-eddy simulation-dedicated experimental database: the pulsatile impinging jet in turbulent cross-flow. *Phys. Fluids* 26:075108, 2014.
 - ³Carlsson, M., E. Heiberg, J. Toger, and H. Arheden. Quantification of left and right ventricular kinetic energy using four-dimensional intracardiac magnetic resonance imaging flow measurements. *AJP Hear. Circ. Physiol.* 302:H893–H900, 2012.
 - ⁴Celik, I. B., Z. N. Cehreli, and I. Yavuz. Index of resolution quality for large eddy simulations. *J. Fluids Eng.* 127:949, 2005.
 - ⁵Charonko, J. J., R. Kumar, K. Stewart, W. C. Little, and P. P. Vlachos. Vortices formed on the mitral valve tips aid normal left ventricular filling. *Ann. Biomed. Eng.* 41:1049–1061, 2013.
 - ⁶Cheng, C. P., D. Parker, and C. A. Taylor. Quantification of Wall shear stress in large blood vessels using Lagrangian interpolation functions with cine phase-contrast magnetic resonance imaging. *Ann. Biomed. Eng.* 30:1020–1032, 2002.

- 753 ⁷Chien, S. Shear dependence of effective cell volume as a
754 determinant of blood viscosity. *Science (80-)* 168:977–979,
755 1970.
- 756 ⁸Chnafa, C. Using image-based large-eddy simulations to
757 investigate the intracardiac flow and its turbulent nature.
758 Montpellier: University of Montpellier, 2014.
- 759 ⁹Chnafa, C., S. Mendez, R. Moreno, and F. Nicoud. Using
760 image-based CFD to investigate the intracardiac turbu-
761 lence. In: *Modeling the Heart and the Circulatory System*,
762 edited by A. Quarteroni. New-York: Springer, 2015, pp.
763 97–117.
- 764 ¹⁰Chnafa, C., S. Mendez, and F. Nicoud. Image-based large-
765 eddy simulation in a realistic left heart. *Comput. Fluids*
766 94:173–187, 2014.
- 767 ¹¹Collins, S. P., P. Arand, C. J. Lindsell, W. F. Peacock, and
768 A. B. Storrow. Prevalence of the third and fourth heart
769 sound in asymptomatic adults. *Congest. Hear. Fail.* 11:242–
770 247, 2005.
- 771 ¹²Davies, P. F., A. Remuzzi, E. J. Gordon, C. F. Dewey, and
772 M. A. Gimbrone. Turbulent fluid shear stress induces
773 vascular endothelial cell turnover in vitro. *Proc. Natl. Acad.*
774 *Sci. USA* 83:2114–2117, 1986.
- 775 ¹³Domenichini, F., G. Pedrizzetti, and B. Baccani. Three-
776 dimensional filling flow into a model left ventricle. *J. Fluid*
777 *Mech.* 539:179, 2005.
- 778 ¹⁴Domenichini, F., G. Querzoli, A. Cenedese, and G. Ped-
779 rizzetti. Combined experimental and numerical analysis of
780 the flow structure into the left ventricle. *J. Biomech.*
781 40:1988–1994, 2007.
- 782 ¹⁵Dyverfeldt, P., M. Bissell, A. J. Barker, A. F. Bolger, C.-J.
783 Carlhäll, T. Ebbers, C. J. Francios, A. Frydrychowicz, J.
784 Geiger, D. Giese, M. D. Hope, P. J. Kilner, S. Kozerke, S.
785 Myerson, S. Neubauer, O. Wieben, and M. Markl. 4D flow
786 cardiovascular magnetic resonance consensus statement. *J.*
787 *Cardiovasc. Magn. Reson.* 17:72, 2015.
- 788 ¹⁶Dyverfeldt, P., M. D. Hope, E. E. Tseng, and D. Saloner.
789 Magnetic resonance measurement of turbulent kinetic en-
790 ergy for the estimation of irreversible pressure loss in aortic
791 stenosis. *JACC Cardiovasc. Imaging* 6:64–71, 2013.
- 792 ¹⁷Dyverfeldt, P., J.-P. E. Kvitting, C. J. Carlhäll, G. Boano,
793 A. Sigfridsson, U. Hermansson, A. F. Bolger, J. Engvall,
794 and T. Ebbers. Hemodynamic aspects of mitral regurgita-
795 tion assessed by generalized phase-contrast MRI. *J. Magn.*
796 *Reson. Imaging* 33:582–588, 2011.
- 797 ¹⁸Dyverfeldt, P., J. P. E. Kvitting, A. Sigfridsson, J. Engvall,
798 A. F. Bolger, and T. Ebbers. Assessment of fluctuating
799 velocities in disturbed cardiovascular blood flow: in vivo
800 feasibility of generalized phase-contrast MRI. *J. Magn.*
801 *Reson. Imaging* 28:655–663, 2008.
- 802 ¹⁹Falahatpisheh, A., and A. Kheradvar. High-speed particle
803 image velocimetry to assess cardiac fluid dynamics in vitro:
804 from performance to validation. *Eur. J. Mech. B/Fluids*
805 35:2–8, 2012.
- 806 ²⁰Glower, D. D., R. L. Murrain, C. O. Olsen, J. W. Davis,
807 and J. S. Rankin. Mechanical correlates of the third heart
808 sound. *J. Am. Coll. Cardiol.* 19:450–457, 1992.
- 809 ²¹Hendabadi, S., J. Bermejo, Y. Benito, R. Yotti, F. Fern-
810 nández-Avilés, J. C. Del Álamo, and S. C. Shadden.
811 Topology of blood transport in the human left ventricle by
812 novel processing of doppler echocardiography. *Ann.*
813 *Biomed. Eng.* 41:2603–2616, 2013.
- 814 ²²Hult, P., T. Fjällbrant, B. Wranne, and P. Ask. Detection
815 of the third heart sound using a tailored wavelet approach.
816 *Med. Biol. Eng. Comput.* 42:253–258, 2004.
- ²³Kanski, M., P. M. Arvidsson, J. Töger, R. Borgquist, E. 817
Heiberg, M. Carlsson, and H. Arheden. Left ventricular 818
fluid kinetic energy time curves in heart failure from car- 819
diovascular magnetic resonance 4D flow data. *J. Cardio- 820*
vasc. Magn. Reson. 17:111, 2015.
- ²⁴Khalafvand, S. S., E. Y. K. Ng, L. Zhong, and T. K. Hung. 821
Fluid-dynamics modelling of the human left ventricle with 822
dynamic mesh for normal and myocardial infarction: pre- 823
liminary study. *Comput. Biol. Med.* 42:863–870, 2012. 824
825
- ²⁵Kheradvar, A., and M. Gharib. On mitral valve dynamics 826
and its connection to early diastolic flow. *Ann. Biomed.* 827
Eng. 37:1–13, 2009. 828
- ²⁶Kilner, P. J., G. Z. Yang, A. J. Wilkes, R. H. Mohiaddin, 829
D. N. Firmin, and M. H. Yacoub. Asymmetric redirection 830
of flow through the heart. *Nature* 404:759–761, 2000. 831
- ²⁷Kono, T., H. Rosman, M. Alam, P. D. Stein, H. N. Sab- 832
bah, D. Stein, and N. Wbbah. Hemodynamic correlates of 833
the third heart sound during the evolution of chronic heart 834
failure. *Am. J. Med.* 21:419–423, 1992. 835
- ²⁸Le, T. B., and F. Sotiropoulos. On the three-dimensional 836
vortical structure of early diastolic flow in a patient-specific 837
left ventricle. *Eur. J. Mech. B/Fluids* 35:20–24, 2012. 838
- ²⁹Long, Q., R. Merrifield, X. Y. Xu, P. Kilner, D. N. Firmin, 839
and G.-Z. Yang. Subject-specific computational simulation 840
of left ventricular flow based on magnetic resonance 841
imaging. *Proc. Inst. Mech. Eng. H* 222:475–485, 2008. 842
- ³⁰Lu, P. C., H. C. Lai, and J. S. Liu. A reevaluation and 843
discussion on the threshold limit for hemolysis in a turbu- 844
lent shear flow. *J. Biomech.* 34:1361–1364, 2001. 845
- ³¹Mann, D. L., D. P. Zipes, P. Libby, and R. O. Bonow. 846
Braunwald's Heart Disease: A Textbook of Cardiovascular 847
Medicine. Philadelphia: Elsevier, p. 2136, 2014. 848
- ³²Markl, M., P. J. Kilner, and T. Ebbers. Comprehensive 4D 849
velocity mapping of the heart and great vessels by cardio- 850
vascular magnetic resonance. *J. Cardiovasc. Magn. Reson.* 851
13:7, 2011. 852
- ³³Mendez, S., E. Gibaud, and F. Nicoud. An unstructured 853
solver for simulations of deformable particles in flows at 854
arbitrary Reynolds numbers. *J. Comput. Phys.* 256:465– 855
483, 2014. 856
- ³⁴Mihalef, V., R. I. Ionasec, P. Sharma, B. Georgescu, I. 857
Voigt, M. Suehling, and D. Comaniciu. Patient-specific 858
modelling of whole heart anatomy, dynamics and haemo- 859
dynamics from four-dimensional cardiac CT images. *In-* 860
terface Focus 1:286–296, 2011. 861
- ³⁵Nicoud, F., H. B. Toda, O. Cabrit, S. Bose, and J. Lee. 862
Using singular values to build a subgrid-scale model for 863
large eddy simulations. *Phys. Fluids* 23:1–35, 2011. 864
- ³⁶Olesen, S. P., D. E. Clapham, and P. F. Davies. Haemo- 865
dynamic shear stress activates a K⁺ current in vascular 866
endothelial cells. *Nature* 331:168–170, 1988. 867
- ³⁷Pasipoularides, A. Diastolic filling vortex forces and car- 868
diac adaptations: probing the epigenetic nexus. *Hell. J.* 869
Cardiol. 53:458–469, 2012. 870
- ³⁸Pasipoularides, A. Mechanotransduction mechanisms for 871
intraventricular diastolic vortex forces and myocardial 872
deformations: part 1. *J. Cardiovasc. Transl. Res.* 8:76–87, 873
2015. 874
- ³⁹Pedrizzetti, G., and F. Domenichini. Left ventricular fluid 875
mechanics: the long way from theoretical models to clinical 876
applications. *Ann. Biomed. Eng.* 43:26–40, 2015. 877
- ⁴⁰Pedrizzetti, G., F. Domenichini, and G. Tonti. On the left 878
ventricular vortex reversal after mitral valve replacement. 879
Ann. Biomed. Eng. 38:769–773, 2010. 880

- 881 ⁴¹Pedrizetti, G., G. La Canna, O. Alfieri, and G. Tonti. The
882 vortex—an early predictor of cardiovascular outcome? *Nat.*
883 *Rev. Cardiol.* 11:545–553, 2014.
- 884 ⁴²Pham, D. L., C. Xu, and J. L. Prince. Current methods in
885 medical image segmentation. *Annu. Rev. Biomed. Eng.*
886 2:315–337, 2000.
- 887 ⁴³Pope, S. B. *Turbulent Flows*. Cambridge: Cambridge
888 University Press, 2000. doi:10.1088/0957-0233/12/11/705.
- 889 ⁴⁴Pope, S. B. Ten questions concerning the large-eddy sim-
890 ulation of turbulent flows. *N. J. Phys.* 6:35, 2004.
- 891 ⁴⁵Querzoli, G., S. Fortini, and A. Cenedese. Effect of the
892 prosthetic mitral valve on vortex dynamics and turbulence
893 of the left ventricular flow. *Phys. Fluids* 22:1–10, 2010.
- 894 ⁴⁶Sabbah, H. N., and P. D. Stein. Turbulent blood flow in
895 humans: its primary role in the production of ejection
896 murmurs. *Circ. Res.* 38:513–525, 1976.
- 897 ⁴⁷Saber, N. R., N. B. Wood, A. D. Gosman, R. D. Merri-
898 field, G. Z. Yang, C. L. Charrier, P. D. Gatehouse, and D.
899 N. Firmin. Progress towards patient-specific computational
900 flow modeling of the left heart via combination of magnetic
901 resonance imaging with computational fluid dynamics.
902 *Ann. Biomed. Eng.* 31:42–52, 2003.
- 903 ⁴⁸Schenkel, T., M. Malve, M. Reik, M. Markl, B. Jung, and
904 H. Oertel. MRI-Based CFD analysis of flow in a human
905 left ventricle: methodology and application to a healthy
906 heart. *Ann. Biomed. Eng.* 37:503–515, 2009.
- ⁴⁹Töger, J., M. Kanski, M. Carlsson, S. J. Kovács, G. 907
Söderlind, H. Arheden, and E. Heiberg. Vortex ring for- 908
mation in the left ventricle of the heart: analysis by 4D 909
Flow MRI and Lagrangian Coherent Structures. *Ann.* 910
Biomed. Eng. 2012. doi:10.1007/s10439-012-0615-3. 911
- ⁵⁰Valen-Sendstad, K., and D. A. Steinman. Mind the gap: 912
impact of computational fluid dynamics solution strategy 913
on prediction of intracranial aneurysm hemodynamics and 914
rupture status indicators. *Am. J. Neuroradiol.* 35:536–543, 915
2014. 916
- ⁵¹Vedula, V., J.-H. Seo, A. C. Lardo, and R. Mittal. Effect of 917
trabeculae and papillary muscles on the hemodynamics of 918
the left ventricle. *Theor. Comput. Fluid Dyn.* 2015. doi: 919
10.1007/s00162-015-0349-6. 920
- ⁵²Watanabe, H., S. Sugiura, and T. Hisada. The looped heart 921
does not save energy by maintaining the momentum of 922
blood flowing in the ventricle. *Am. J. Physiol. Heart Circ.* 923
Physiol. 294:H2191–H2196, 2008. 924
- ⁵³Zajac, J., J. Eriksson, P. Dyverfeldt, A. F. Bolger, T. Eb- 925
bers, and C.-J. Carlhäll. Turbulent kinetic energy in normal 926
and myopathic left ventricles. *J. Magn. Reson. Imaging* 927
41:1021–1029, 2015. 928

UNCORRECTED PROOF